F-Actin Dynamics in Neurospora crassa

EUKARYOTIC CELL, Apr. 2010, p. 547–557 Vol. 9, No. 4
1535-9778/10/$12.00 doi:10.1128/EC.00253-09

F-Actin Dynamics in *Neurospora crassa*▽†

Adokiye Berepiki,[1]§ Alexander Lichius,[1]§ Jun-Ya Shoji,[1] Jens Tilsner,[2] and Nick D. Read[1]*

Fungal Cell Biology Group, Institute of Cell Biology, University of Edinburgh, Rutherford Building, Edinburgh EH9 3JH, United Kingdom,[1] and Scottish Crop Research Institute, Invergowrie, Dundee DD2 5DA, United Kingdom[2]

Received 28 August 2009/Accepted 29 January 2010

This study demonstrates the utility of Lifeact for the investigation of actin dynamics in *Neurospora crassa* and also represents the first report of simultaneous live-cell imaging of the actin and microtubule cytoskeletons in filamentous fungi. Lifeact is a 17-amino-acid peptide derived from the nonessential *Saccharomyces cerevisiae* actin-binding protein Abp140p. Fused to green fluorescent protein (GFP) or red fluorescent protein (TagRFP), Lifeact allowed live-cell imaging of actin patches, cables, and rings in *N. crassa* without interfering with cellular functions. Actin cables and patches localized to sites of active growth during the establishment and maintenance of cell polarity in germ tubes and conidial anastomosis tubes (CATs). Recurrent phases of formation and retrograde movement of complex arrays of actin cables were observed at growing tips of germ tubes and CATs. Two populations of actin patches exhibiting slow and fast movement were distinguished, and rapid (1.2 μm/s) saltatory transport of patches along cables was observed. Actin cables accumulated and subsequently condensed into actin rings associated with septum formation. F-actin organization was markedly different in the tip regions of mature hyphae and in germ tubes. Only mature hyphae displayed a subapical collar of actin patches and a concentration of F-actin within the core of the Spitzenkörper. Coexpression of Lifeact-TagRFP and β-tubulin–GFP revealed distinct but interrelated localization patterns of F-actin and microtubules during the initiation and maintenance of tip growth.

Actins are highly conserved proteins found in all eukaryotes and have an enormous variety of cellular roles. The monomeric form (globular actin, or G-actin) can self-assemble, with the aid of numerous actin-binding proteins (ABPs), into microfilaments (filamentous actin, or F-actin), which, together with microtubules, form the two major components of the fungal cytoskeleton. Numerous pharmacological and genetic studies of fungi have demonstrated crucial roles for F-actin in cell polarity, exocytosis, endocytosis, cytokinesis, and organelle movement (6, 7, 20, 34, 35, 51, 52, 59). Phalloidin staining, immunofluorescent labeling, and fluorescent-protein (FP)-based live-cell imaging have revealed three distinct subpopulations of F-actin-containing structures in fungi: patches, cables, and rings (1, 14, 28, 34, 60, 63, 64). Actin patches are associated with the plasma membrane and represent an accumulation of F-actin around endocytic vesicles (3, 26, 57). Actin cables are bundles of actin filaments stabilized with cross-linking proteins, such as tropomyosins and fimbrin, and are assembled by formins at sites of active growth, where they form tracks for myosin V-dependent polarized secretion and organelle transport (10, 16, 17, 27, 38, 47, 48). Cables, unlike patches, are absolutely required for polarized growth in the budding yeast *Saccharomyces cerevisiae* (34, 38). Contractile actomyosin rings are essential for cytokinesis in budding yeast, whereas in filamentous fungi, actin rings are less well studied but are known to be involved in septum formation (20, 28, 34, 39, 40).

Actin cables and patches have been particularly well studied in budding yeast. However, there are likely to be important differences between F-actin architecture and dynamics in budding yeast and those in filamentous fungi, as budding yeasts display only a short period of polarized growth during bud formation, which is followed by isotropic growth over the bud surface (10). Sustained polarized growth during hyphal morphogenesis is a defining feature of filamentous fungi (21), making them attractive models for studying the roles of the actin cytoskeleton in cell polarization, tip growth, and organelle transport.

In *Neurospora crassa* and other filamentous fungi, disruption of the actin cytoskeleton leads to rapid tip swelling, which indicates perturbation of polarized tip growth, demonstrating a critical role for F-actin in targeted secretion to particular sites on the plasma membrane (7, 22, 29, 56). Immunofluorescence studies of *N. crassa* have shown that F-actin localizes to hyphal tips as "clouds" and "plaques" (7, 54, 59). However, immunolabeling has failed to reveal actin cables in *N. crassa* and offers limited insights into F-actin dynamics. Live-cell imaging of F-actin architecture and dynamics has not been accomplished in *N. crassa*, yet it is expected to yield key insights into cell polarization, tip growth, and intracellular transport.

We took advantage of a recently developed live-cell imaging probe for F-actin called Lifeact (43). Lifeact is a 17-amino-acid peptide derived from the N terminus of the budding yeast actin-binding protein Abp140 (5, 63) and has recently been demonstrated to be a universal live-cell imaging marker for F-actin in eukaryotes (43). Here, we report the successful application of fluorescent Lifeact fusion constructs for live-cell imaging of F-actin in *N. crassa*. We constructed two synthetic genes consisting of Lifeact fused to "synthetic" green fluores-

* Corresponding author. Mailing address: Fungal Cell Biology Group, Institute of Cell Biology, University of Edinburgh, Rutherford Building, Edinburgh EH9 3JH, United Kingdom. Phone: 44-131-650-5335. Fax: 44-131-650-5392. E-mail: Nick.Read@ed.ac.uk.

§ A.B. and A.L. contributed equally to this work.

† Supplemental material for this article may be found at http://ec.asm.org/.

▽ Published ahead of print on 5 February 2010.

cent protein (sGFP) (S65T) (henceforth termed GFP) (12) or red fluorescent protein (TagRFP) (33) and expressed these constructs in various *N. crassa* strains. In all strain backgrounds, fluorescent Lifeact constructs clearly labeled actin patches, cables, and rings and revealed a direct association of F-actin structures with sites of cell polarization and active tip growth. Our results demonstrate the efficacy of Lifeact as a nontoxic live-cell imaging probe in *N. crassa*.

MATERIALS AND METHODS

Strains and culture conditions. The *N. crassa* strains generated during this study were derived from FGSC 4200 (wild type [WT] *mat a*), FGSC 2489 (WT *mat A*), FGSC 9717 (*mat A his-3* Δ*mus-51*::*bar*$^+$), and FGSC N2506 (*mat a* β-*tubulin rid his-3*$^+$::*bml-gfp*) strains obtained from the Fungal Genetics Stock Center (FGSC) (School of Biological Sciences, Kansas City, MO). Five strains were constructed: NCAB1721 (*mat A his-3*$^+$::*Pccg-1-Lifeact-gfp* Δ*mus-51*::*bar*$^+$), NCAB1761 (*mat A his-3*$^+$::*Ptef-1-Lifeact-gfp* Δ*mus-51*::*bar*$^+$), NCAL004 (*mat a Pccg-1-Lifeact-tagrfp*::*bar*$^+$), NCAL005 (*mat A Pccg-1-Lifeact-tagrfp*::*bar*$^+$), and NCAL006 (*mat a* β-*tubulin rid his-3*$^+$::*bml-gfp*; *Pccg-1-Lifeact-tagrfp*::*bar*$^+$). The strains were maintained on Vogel's minimal medium (VMM) with 2% sucrose, and all manipulations were performed according to standard *N. crassa* techniques (13).

Plasmid construction. To visualize Lifeact-GFP in *N. crassa*, we constructed a synthetic gene for integration at the *his-3* locus. To construct the Lifeact-GFP plasmid, we designed the *N. crassa* codon-optimized oligonucleotides 5′-GATC TCTAGAATGGGCGTCGCTGACCTCATCAAGAAGTTCGAGTCCATCT CCAAGGAGGAGTTAATTAACTAG-3′ and 5′-CTAGTTAATTAACTCCT CCTTGGAGATGGACTCGAACTTCTTGATGAGGTCAGCGACGCCCAT TCTAGAGATC-3′, which contained the Lifeact sequence, an XbaI site (underlined) at one end, and a PacI site (underlined) at the other end. After being boiled for 5 min, the oligonucleotides were incubated at room temperature for 30 min to anneal them and then digested with XbaI and PacI and inserted into an XbaI- and PacI-digested GFP expression vector, pCCG-1::C-Gly::GFP (24) (obtained from the FGSC), yielding pAB221.

We found that expression of the Lifeact construct from the *ccg-1* promoter did not allow satisfactory visualization of Lifeact-GFP in mature vegetative hyphae. Therefore, the 0.9-kb upstream regulatory region of the *N. crassa* locus NCU02003 (transcriptional elongation factor 1 homolog, *tef-1*) was amplified by PCR and exchanged for *Pccg-1* in the pAL1 GFP expression vector, yielding pTEFsG-2. Following confirmation that the putative *tef-1* promoter provided GFP expression throughout the *N. crassa* life cycle (data not shown), the *Ptef-1* sequence was amplified from pTEFsG-2 using the primers 5′-ACCGCGGTGG CGGCCGCGATATCCCGTGACCACTGAACTA-3′ and 5′-CGACGCCCAT TCTAGATAACCCGGGGATCCGATAT-3′ and integrated into NotI- and XbaI-digested pAB221 using the In-Fusion PCR cloning kit (Clontech, Mountain View, CA), yielding pAB261.

To facilitate dual-labeling studies, we developed a Lifeact-TagRFP fusion construct. A Lifeact-TagRFP fusion was made from the plasmid pGWB460 (T. Nakagawa, Shimane University, Matsue, Japan, unpublished data), which contains the TagRFP (33) open reading frame. TagRFP was altered by the addition of N- and C-terminal amino acids from GFP, increasing its utility for four-dimensional (4D) live-cell imaging (49). TagRFP-specific codons (in italics) and the Lifeact sequence (underlined) were added by PCR using the oligonucleotides 5′-ATGGGTGTCGCAGATTTGATCAAGAAATTCGAAAGCATCTCAAA GGAAGAAGGCTCG*ATGGTGTCTAAGGGCGAA*GAGCTGATTAAGGA GAACATGCAC-3′ and 5′-*TTACTTGTACAGCTCGTCCATGCCATTAAG*TT TGTGCCCCAGTTTGCTAG-3′. In contrast to the Lifeact-GFP construct, the Lifeact sequence in the Lifeact-TagRFP fusion protein was not codon optimized for *N. crassa*. The Lifeact-TagRFP expression vector pAL3-Lifeact was constructed by amplifying the resulting 821-bp fragment encoding Lifeact-TagRFP using the primers 5′-TTTCCTCGACGGATCCATGGGTGTCGCAGATTTG ATCAAGA-3′ and 5′-ATCGATAAGCTTGATATCTTACTTGTACAGCTCG TCCATGCCA-3′ and integrating the purified PCR product into BamHI- and EcoRV-digested pBARGRG1 (36) using the In-Fusion PCR cloning kit (Clontech). DNA sequencing was carried out on all vectors to confirm in-frame cloning of the fusion constructs. Thus, Lifeact-GFP constructs were expressed under the control of the *ccg-1* or *tef-1* promoter and consisted of the Lifeact sequence fused to GFP at its C terminus via a 10-glycine linker, whereas the Lifeact-TagRFP construct was expressed under the control of the *ccg-1* promoter and consisted of the Lifeact sequence fused to TagRFP at its C terminus via a 2-amino-acid (GS) linker.

Transformation and transformant selection. Transformations were performed as described previously (32). To generate strains expressing Lifeact-GFP, NdeI-digested pAB221 and pAB261 were targeted to the *his-3* locus of strain FGSC 9717 (*mat A his-3* Δ*mus-51*::*bar*$^+$). Lifeact-TagRFP-expressing strains were created by introducing pAL3-Lifeact into strains FGSC 4200 (WT *mat a*), FGSC 2489 (WT *mat A*), and FGSC N2506 (*mat a* β-*tubulin rid his-3*$^+$::*bml-gfp*). Transformants were selected either by recovery of histidine prototrophy or on nitrogen-free VMM containing the Ignite (phosphinothricin) selection marker. Southern blotting using a DIG High Prime DNA Labeling and Detection Starter Kit (Roche Diagnostics, Mannheim, Germany), along with a PCR DIG Probe Synthesis Kit (Roche Diagnostics), was performed to check the genotypes of the transformants (see Fig. S1A in the supplemental material).

Lifeact-GFP and Lifeact-TagRFP expression was examined in multiple transformants using a Nikon SMZ1500 stereomicroscope with a GFP (excitation, 470/40 nm; 505-nm long pass dichroic mirror; emission, 530/40 nm) or RFP (excitation, 545/30 nm; 570-nm long pass dichroic mirror; emission, 620/60 nm) filter set. Intracellular expression patterns were analyzed in at least nine transformants per plasmid construct by wide-field fluorescence microscopy. Transformants exhibiting FP expression were selected for subsequent live-cell imaging studies.

Live-cell imaging. Conidia were collected from 3- to 5-day-old cultures and suspended in VMM. In all experiments, unless stated otherwise, conidia were used at a concentration of 10^6 cells per ml. The cells were incubated in VMM in Lab-Tek 8-well chamber slides (Nalge-Nunc International, Rochester, NY) for 2 to 4 h at 35°C and then imaged. To image mature hyphae, conidia were grown in petri dishes containing VMM solidified with 1.5% agar for 16 to 20 h at 24°C and then prepared for imaging using the "inverted agar block method" (23). Imaging was carried out at room temperature. The images were collected using a DeltaVision microscope (Applied Precision, Issaquah, WA) consisting of an Olympus IX70 base, an Olympus 100×/1.4-numerical-aperture (NA) Plan-Apo objective, a 75-W HBO illuminator; a Chroma Sedat Quad ET filter set (for GFP, excitation = 490/20 nm, emission = 528/38 nm; for RFP, excitation = 545/30 nm, emission = 610/75 nm; for FM4-64, excitation = 490/20 nm, emission = 685/40 nm; for calcofluor white, excitation = 360/40 nm, emission = 457/50 nm; Chroma Technology Corp., Rockingham, VT), a CoolSnap HQ charge-coupled-device (CCD) camera (Photometrics, Tuscon, AZ), and SoftWorx software (Applied Precision) for image acquisition. Exposure times ranged from 200 to 400 ms. To acquire 3D (x, y, z) images, 30 to 40 optical sections were obtained at 0.2-μm steps. For 4D imaging (x, y, z, and t), 10 to 15 optical sections were obtained at 0.4- or 0.5-μm steps and 30- to 120-s intervals. The images were processed through 10 iterative deconvolutions using SoftWorx image analysis software. To image actin patch dynamics, time-lapse sequences were captured in one focal plane using 2 × 2 camera binning at 200- to 300-ms intervals. Extension rates, patch velocities, and lifetimes were measured manually using the track object function of the Image Pro-Plus analysis software (version 7.0; Media Cybernetics, Bethesda, MD). The (x, y) coordinates of individual patches or hyphal tips were recorded, and the velocities of objects were calculated as the sum of the distance between points divided by time. The velocities of individual patches were averaged to obtain the mean velocity. Patch lifetimes were determined by multiplying the frame interval by the number of frames in which an individual patch was visible before it moved out of the focal plane. The size of the F-actin-depleted zone was determined using the measurement option of Image Pro-Plus. Projections and further processing steps were carried out with ImageJ software (http://rsbweb.nih.gov/ij/). Some single-plane time-lapse (x, y, t) sequences were processed with an "unsharp mask" filter to aid visualization of fine cytoskeletal details.

Fluorescent staining. Mature hyphae and germlings were labeled for 30 min with either 2 μM FM4-64 (prepared from 200 μM stock in dimethyl sulfoxide [DMSO]; Molecular Probes, Eugene, OR), which stains the plasma membrane and organelle membranes (18, 23), or 0.1 μg/ml calcofluor white (prepared from 1 mg/ml stock in ethanol; Sigma, Welwyn Garden City, United Kingdom), which stains cell walls (23).

Latrunculin A treatment. Latrunculin A (Lat A) (Invitrogen, Carlsbad, CA) was stored as a 1 mM stock in DMSO. For Lat A treatment of growing cells, 25 μl of growth medium was removed from the observation chamber and replaced with 25 μl of medium supplemented with an appropriate volume of the Lat A stock solution or DMSO. Lat A was used at a final concentration of 10 μM. To quantify the effect of Lat A on the presence of patches and cables, cells were incubated in Lab-Tek 8-well chamber slides for 4 h in 250 μl of VMM at a concentration of 10^6 cells/ml. The effect of Lat A treatment was monitored with time-lapse microscopy 1 min after its addition. Cells were scored for the presence

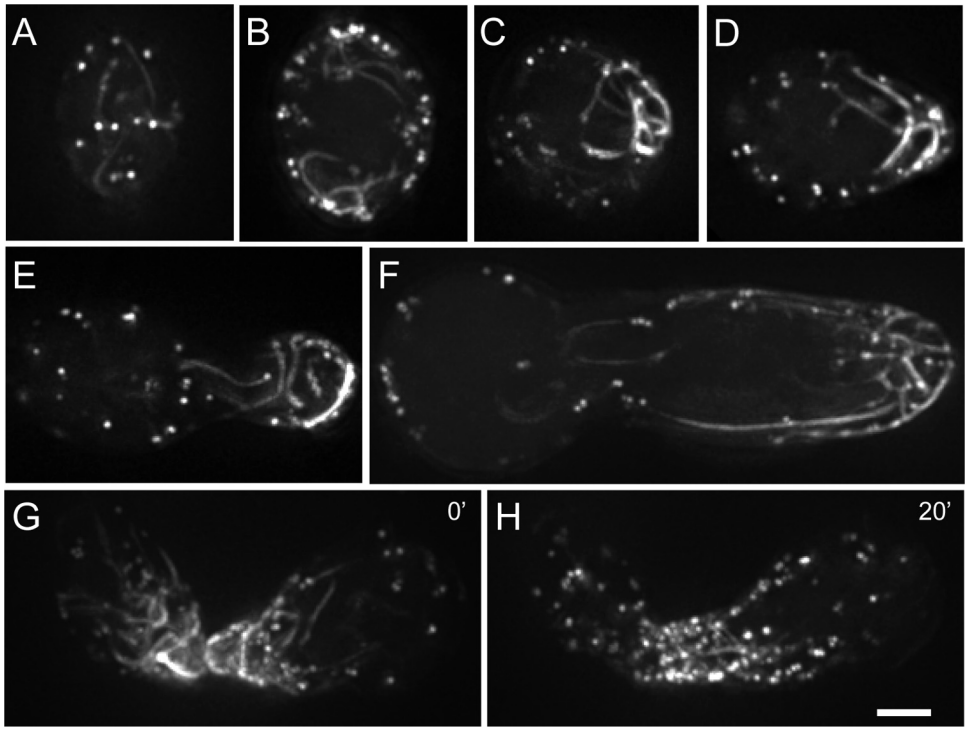

FIG. 1. Lifeact-GFP localization during germ tube emergence and CAT-mediated cell fusion. Maximum-intensity projections of 5 to 10 planes of different conidia at various stages of development are shown. (A and B) Maximum-intensity projections of 6 optical planes from the top (A) and middle (B) of an ungerminated spore. Actin patches and cables are mostly associated with the cell cortex. (C and D) A meshwork-like actin array always marks the site of germ tube emergence. (E, F, and G) Actin arrays persist at sites of active growth. (F) Long actin cables extend longitudinally through the germ tube. (G and H) Maximum-intensity projections of a time-lapse sequence showing enrichment of cables and patches at CAT tips before cell fusion (G) and loss of actin cables after fusion (H). Bar, 2 μm.

or absence of patches or cables at 1-min intervals by visual inspection of time-lapse sequences.

RESULTS

Lifeact-GFP and Lifeact-TagRFP label F-actin in *N. crassa*. We visualized F-actin in *N. crassa* by expressing Lifeact-GFP or Lifeact-TagRFP under the control of the *ccg-1* or *tef-1* promoter. All clones chosen for live-cell imaging studies grew, germinated, and fused at wild-type rates, were healthy and conidiated normally at 25°C and 35°C, and possessed colony morphologies similar to that of the wild type (see Fig. S1 in the supplemental material). Lifeact-TagRFP gave a pattern of actin localization identical to that of Lifeact-GFP and had comparable brightness and photostability. Henceforth, we refer to Lifeact-GFP or Lifeact-TagRFP interchangeably as Lifeact-FP.

To image Lifeact-FP, we used wide-field fluorescence microscopy combined with image deconvolution. Lifeact-FP gave robust labeling of actin patches, cables, and rings (Fig. 1; also see Fig. 5) and displayed a localization pattern of F-actin consistent with previous studies of *N. crassa* using immunofluorescent labeling (7, 22, 54, 59). Latrunculin A treatment, which disrupts the actin cytoskeleton, confirmed F-actin labeling (see below).

F-actin localizes in complex arrays during the establishment and maintenance of polarized growth. Three distinct phases are associated with conidial germination leading to germ tube formation: (i) hydration and isotropic growth, (ii) germ tube emergence, and (iii) germ tube extension (4, 21). During isotropic growth, actin cables were unpolarized and mostly associated with the cell cortex (Fig. 1A and B). Similarly, actin patches were found at the cell periphery but showed no accumulation at particular sites in ungerminated conidia. Prior to germ tube emergence, we observed a strong accumulation of fluorescence that formed a polar cap marking the site of germination (Fig. 1C). Individual cables in this highly dynamic array of F-actin were generally not oriented along the future longitudinal axis but rather followed the curvature of the polarizing cell (Fig. 1C and D). In some instances, this cap disappeared and reformed at a different site on the cell cortex, suggesting that the axis of polarity had not been stably established.

In growing germ tubes, actin cables were mostly found at the cell cortex and organized longitudinally throughout the length of the cell, terminating in a dense meshwork-like array at growing tips (Fig. 1E and F). We commonly observed long (5- to 10-μm) actin cables in germ tubes (Fig. 1F). Occasionally, cables that spanned the entire length of a 25-μm germ tube were visible (see Fig. S2 in the supplemental material). Cortical actin patches were present along the whole length of germ tubes, although, as with cables, they were concentrated at sites of active growth. These observations indicate a close association of actin patches and actin cable arrays with active tip growth. We often observed colocalization of patches and ca-

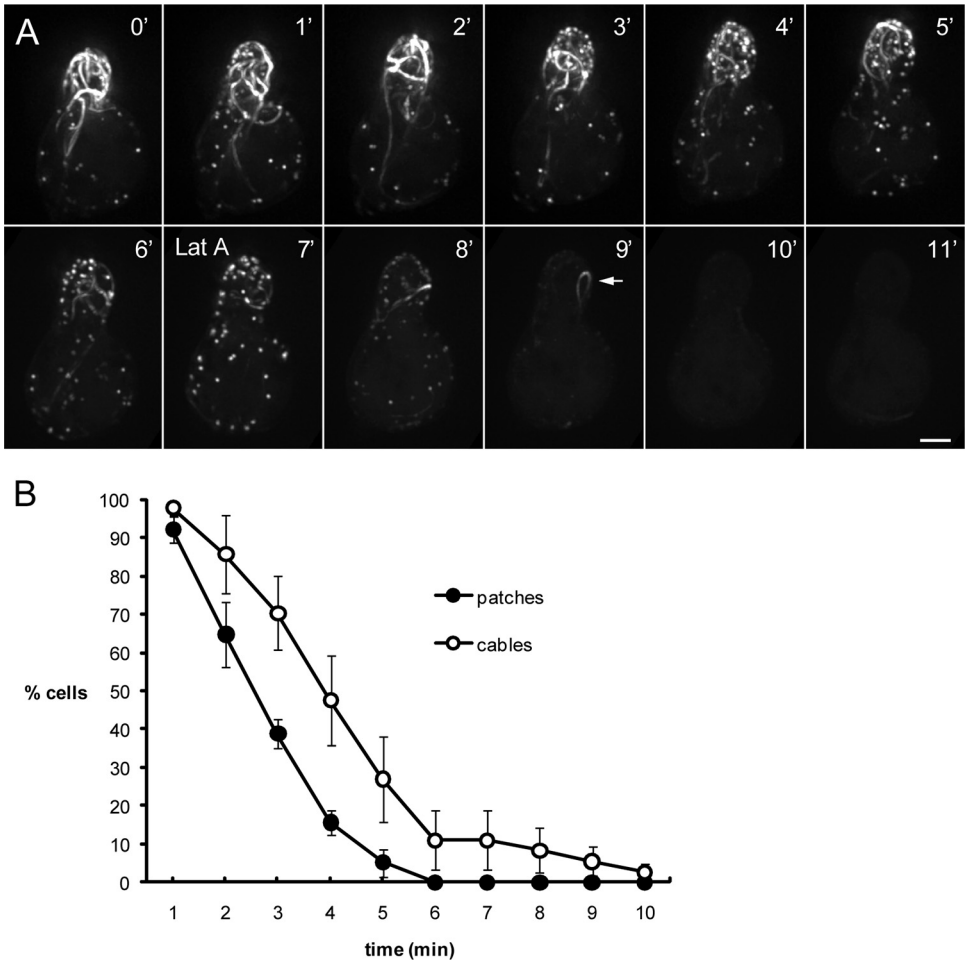

FIG. 2. Lifeact-GFP localization is sensitive to latrunculin A. Growing germ tubes of *N. crassa* were treated with 10 μM Lat A dissolved in DMSO. (A) Maximum-intensity projections of a time-lapse sequence of an elongating germ tube before and after Lat A treatment. Eleven minutes of the full 25-min sequence is shown. Lat A was added at the 7-min (7′) time point and caused a loss of Lifeact-GFP-labeled structures within 4 min. The arrow at the 9-min time point shows a cable that is not tethered to a particular site. The extension rate in the 10 min before Lat A addition was 0.24 μm/min. Following treatment, the extension rate was reduced to 0.005 μm/min. Incubation with an equivalent amount of DMSO (1%) had no effect on Lifeact-GFP localization (not shown). (B) Percentages of cells containing actin patches and actin cables after treatment with 10 μM Lat A (n = 39 cells). Bar, 2 μm. The error bars indicate standard deviations.

bles at the cell periphery and occasionally observed movement of patches along the length of a cable (see below and Fig. 4A and B; see Movie S5 in the supplemental material). The germ tubes analyzed in this study had extension rates of 0.05 to 1.5 μm/min (n = 30).

Latrunculin A caused a rapid loss of Lifeact-FP-labeled structures. Although the Lifeact-FP localization observed here was consistent with previous reports of F-actin distribution in yeast and filamentous fungi, we confirmed the F-actin specificity of the probe using latrunculin A. Latrunculins are potent inhibitors of F-actin polymerization and have been shown to cause rapid disruption of the actin cytoskeleton in fungi (6, 22, 29, 37, 55, 63). We monitored F-actin dynamics in a growing germ tube for 10 min before and after the addition of 10 μM Lat A (Fig. 2A). We found that treatment with Lat A led to a rapid loss of Lifeact-FP fluorescence associated with patches and cables. This confirmed that Lifeact-FP binds to F-actin in *N. crassa*. Germ tube elongation was abrogated by Lat A, emphasizing the importance of F-actin for tip growth (Fig. 2A). Interestingly, upon treatment with Lat A, we occasionally observed a subpopulation of cables that did not appear to be tethered to a particular site (Fig. 2A, arrow at 9 min) and displayed random motion. These cables eventually disassembled, but their initial insensitivity to Lat A showed that the rates of F-actin depolymerization varied within the population of cables. Quantification of the presence of patches and cables following Lat A treatment showed that patches were more sensitive to Lat A, with 83% of cells lacking patches after 4 min compared to 52% of cells lacking cables (n = 39 germlings) (Fig. 2B). Assuming that Lat A only affects actin polymerization (6), this finding also indicates that complete turnover of F-actin in patches and most cables occurs within 4 to 6 min, with cables generally having a longer half-life.

Retrograde movement of actin arrays accompanies polarized growth. Actin cables have been shown to be highly dynamic structures in budding yeast (63). In *N. crassa*, the actin cytoskeleton was in a constant state of flux, with individual actin cables displaying regular kinking and buckling along their

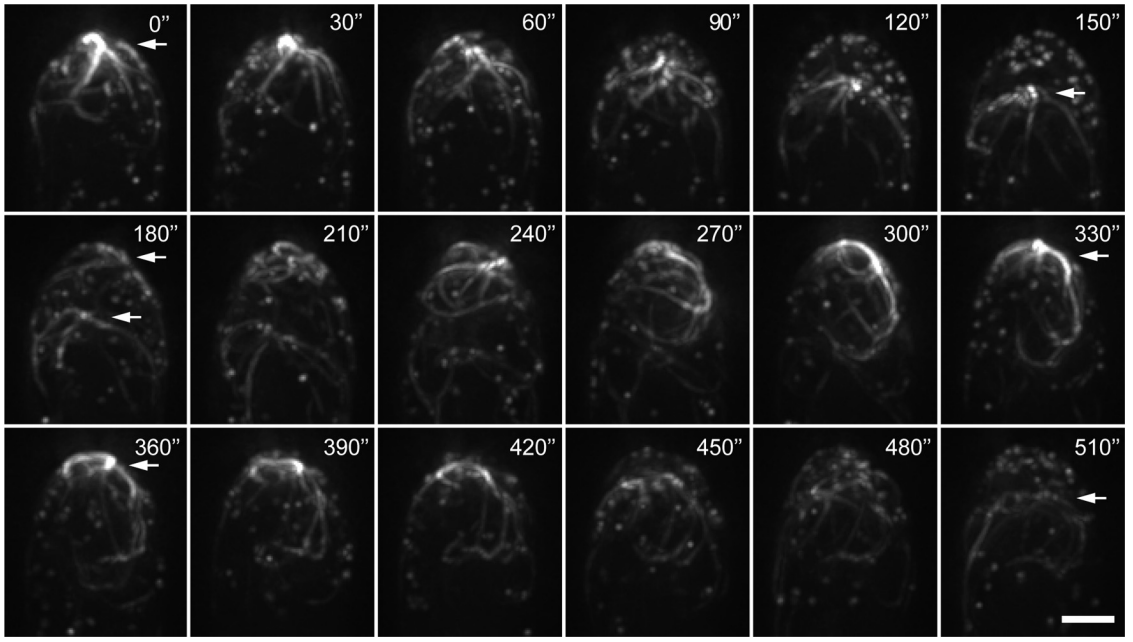

FIG. 3. Retrograde movement of actin cables during germ tube elongation. Maximum-intensity projections of a time-lapse series show actin cable dynamics. The arrow at the 0-s (0″) time point shows an actin array characterized by a bright focal point with cables emanating from it. At the 60-s time point, the actin array started to move back, and by 180 s, the array was no longer present at the germ tube tip. At the 180-s time point, a new actin array (upper arrow) had begun to form, and it subsequently underwent retrograde movement from the tip, as can be seen at the 510-s time point. The extension rate of the germling was 0.18 μm/min. Bar, 2 μm. (See Movies S2 and S3 in the supplemental material.)

lengths. We also observed numerous transient cable-cable interactions and the apparent "exploratory" movement of the untethered ends of individual cables after they were detached or severed (see Movie S1 in the supplemental material).

Another striking aspect of cable dynamics was observed during germ tube emergence and elongation (after 2 to 4 h of incubation). Actin arrays were associated with sites of polarized growth in germlings; intriguingly, these arrays were not static but formed within germ tube tips and underwent recurrent retrograde movement from the elongating tips (Fig. 3). This behavior was commonly observed during germ tube elongation but not during tip extension in mature hyphae (see below and Movies S2, S3, and S4 in the supplemental material). The whole process of actin array formation, retrograde movement, and dissolution generally occurred over a 2- to 10-min period.

Given the dynamic nature of actin cables, we attempted to measure the extension rate of cables from the tips. Yang and Pon (63) used "fiduciary" marks on actin cables to assess cable extension rates. We were unable to find similar stable reference points suitable for such analysis, and generally, quantitative analysis was hindered by the complicated architecture of actin arrays and their highly irregular movements. However, it was apparent that array formation involved the polymerization of cables and that cable extension pushed back the array while tip growth was occurring (see Movies S2 and S3 in the supplemental material).

Actin patches exhibit different types of behavior. Actin patches were visualized throughout the lengths of germlings but were concentrated at sites of active growth. Due to the extremely rapid movement of actin patches, time-lapse observations of patch dynamics were limited to a single focal plane. Consistent with reports on other fungi (3, 26, 37, 55, 57), in *N. crassa*, two types of actin patch movement could be distinguished: slow/nonlinear and fast/linear (Fig. 4; see Movie S5 in the supplemental material). Slow/nonlinear patches formed at the plasma membrane and, following a short period of undirected movement, tracked along actin cables and left the plane of focus, presumably moving to the interior of the cell (Fig. 4A). The mean velocity and lifetime of slow/nonlinear patches were determined to be 0.26 ± 0.08 μm/s and 14 s (n = 23; 6 germlings), respectively. In contrast, the mean velocity of fast/linear patches was 1.2 ± 0.21 μm/s (n = 14; 4 germlings). Fast/linear movement of patches was discontinuous and occurred along the lengths of actin cables, with patches traveling toward and away from the growing tip (Fig. 4B). In some instances, actin patches appeared on the plasma membrane and subsequently underwent directed linear movement along actin cables (see Movie S5 in the supplemental material).

Actin rings assemble prior to septum formation. We monitored the formation and dissipation of actin rings with Lifeact-FP (Fig. 5). Dual labeling with Lifeact-GFP and the cell wall stain calcofluor white showed that ring formation preceded septum formation and that as the septum matured the actin ring was cleaved into two separate accumulations of F-actin and eventually dissipated (Fig. 5A). The duration from initiation to dissipation varied between 30 and 60 min. Formation of these rings occurred by an initially loose accumulation of actin cables in a small area of the hypha, which gradually condensed and shaped itself into an actin ring (see Movie S6 in the supplemental material). Actin cables did not persist around

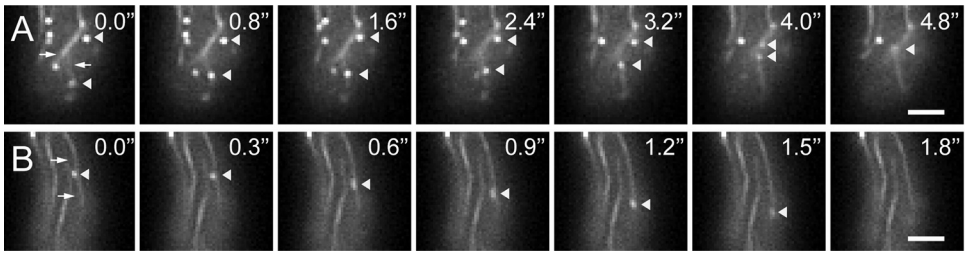

FIG. 4. Actin patches show close association with actin cables. The movement of Lifeact-GFP-labeled patches was monitored by time-lapse microscopy in a single focal plane. (A) Patches (arrowheads) formed at the plasma membrane exhibited a short period of slow/nonlinear movement and then tracked along actin cables (arrows) out of the plane of focus. (B) Fast/linear movement of an actin patch (arrowhead) along an actin cable (arrows). Bars, 2 μm.

the newly formed ring but appeared to be incorporated into its structure (Fig. 5B).

F-actin localization in mature hyphae is distinct from that in germ tubes. Lifeact-FP revealed marked differences in F-actin localization between the tip regions of mature hyphae and germ tubes. In mature hyphae, we observed a concentrated spot of F-actin at the extreme apices of hyphal tips, followed by an F-actin-depleted zone and a collar of actin patches 3.51 ± 1.21 μm ($n = 15$) from the F-actin spot (Fig. 6). The F-actin exclusion zone and spot were present in all actively growing mature hyphae that were observed ($n = 27$). We used the membrane-selective dye FM4-64 to determine whether the F-actin spot localized to the Spitzenkörper (Spk). The Spk is readily stained by FM4-64 and localizes to the tip region of actively growing mature hyphae (18, 23) but is absent from sites of polarized growth in germlings of *N. crassa* (4). Lifeact-FP/FM4-64 colabeling demonstrated that the F-actin spot localized to the core of the Spk, indicating that this may be a center for F-actin organization (Fig. 6B). Notably, actin cables were not visualized in the tip regions of actively growing mature hyphae, although we did observe an accumulation of cables prior to branch formation (Fig. 6C). Cables were present in the new branch for a short period (<10 min), after which the F-actin spot and collar of patches developed and the branches had achieved a linear rate of extension. The leading mature hyphae analyzed in this study exhibited extension rates of 9.1 to 12.4 μm/min ($n = 15$).

Coexpression of Lifeact-TagRFP and β-tubulin–GFP revealed distinct spatial organizations of F-actin and microtubules. In order to investigate the spatial relationship between F-actin and microtubules, we constructed a strain expressing Lifeact-TagRFP and β-tubulin–GFP. Both marker proteins accurately labeled their intended target polymers and showed no nonspecific background staining, cross excitation, or emission bleedthrough (see Movie S7 in the supplemental material). Our initial findings showed that F-actin and microtubules were distinctively organized in conidia and germlings of *N. crassa* (Fig. 7). We commonly observed regions within germlings occupied by F-actin that contained no or only very few microtubules (germ tube a in Fig. 7C), as well as the opposite situation, where microtubules extended into a germ tube tip in which F-actin arrays were absent (germ tube b in Fig. 7C). Recruitment of F-actin to the cell cortex during polarity estab-

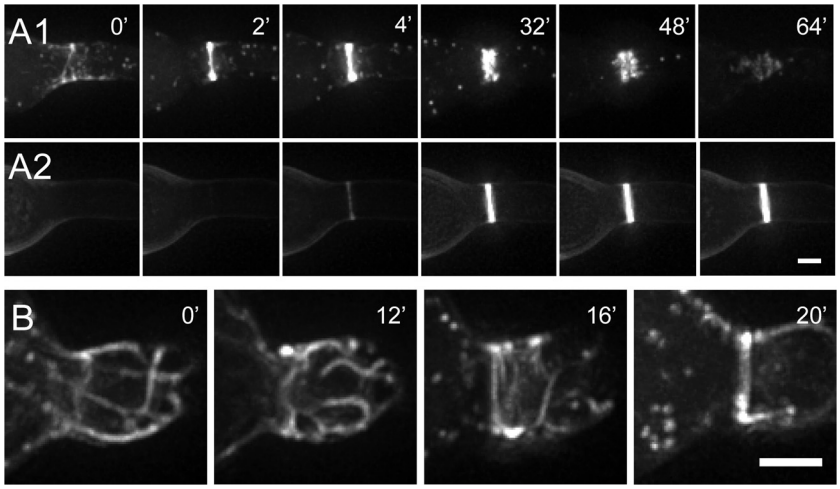

FIG. 5. Actin cables condense to form actin rings. (A1 and A2) Maximum-intensity projections of a time-lapse series showing Lifeact-FP (A1) and calcofluor white (A2) localization during septation. A septum was formed after the appearance of an actin ring. Ring cleavage was visible at the 48-min time point, and F-actin gradually dissipated thereafter. (B) Maximum-intensity projections of a time-lapse series showing actin ring formation. A dense network of actin cables is visible around the future site of ring formation between the 0- and 12-min time points. At 16 min, the cables gradually condensed into an actin ring, which was fully formed 4 min later. Bars, 2 μm.

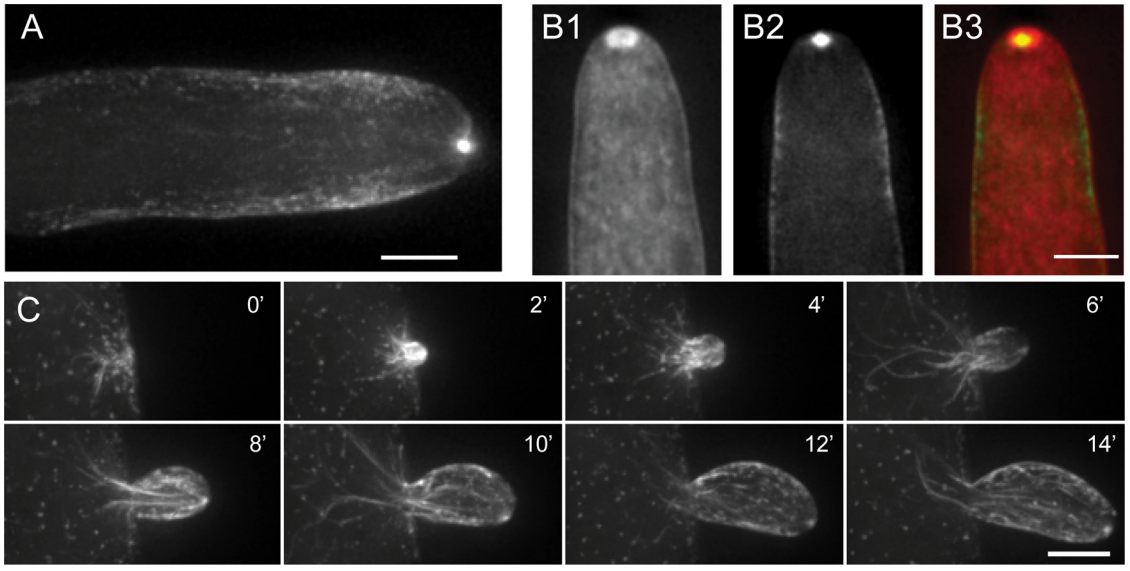

FIG. 6. Lifeact-GFP localization in mature hyphae. (A) Maximum-intensity projection of a hyphal tip. F-actin is concentrated in a spot at the tip, and patches are localized in a subapical collar around the hypha. (B1, B2, and B3) Lifeact-GFP and FM4-64 colabeling of a hyphal tip. (B1) FM4-64. (B2) Lifeact-GFP. (B3) Merged image of both channels with Lifeact-GFP in green and FM4-64 in red. Lifeact-GFP localized to the core of the Spitzenkörper and is shown in yellow where it colocalized with FM4-64. (C) Maximum-intensity projections of a time-lapse sequence showing branch formation. Actin cables were present during early stages of branch outgrowth, but F-actin organization changed as the new branch developed. Bars, 5 μm.

lishment was not accompanied by accumulation of microtubules at that site (ungerminated conidium c in Fig. 7C).

Actin organization during CAT formation is similar to that in germ tube emergence. Conidial anastomosis tubes (CATs) formed by conidia and germ tubes are attracted to and fuse with other CATs to form a germling network (41, 42, 45). The organization of F-actin during CAT formation was in general very similar to that observed during germ tube initiation and outgrowth (see Movie S8 in the supplemental material). CAT formation also coincided with localized accumulation of F-actin at the cell cortex and protrusion of a small bud (Fig. 8, arrowheads). An apical actin cap formed at the bud tip and remained present during CAT extension but eventually disappeared (Fig. 8G to I), suggesting that the CAT had stopped growing as it reached its determinate length (45). In the observed cell, CAT formation coincided with the transient dissolution of the F-actin array present at the germ tube tip (Fig. 8D to H, arrow) and coincided with a decrease in the tip extension rate. In neighboring cells that did not form CATs, actin arrays remained present at the germ tube tips throughout the time course (Fig. 8).

Actin arrays localize to CAT tips during homing and disappear after fusion but are redeployed during germ tube repolarization. During CAT-mediated cell fusion, we found that actin cables and patches localized to CAT tips (Fig. 1G and 9). When two CATs were homing toward each other, equal accumulations of fluorescence in both cell protrusions was typically observed. If only one of the interacting CATs was growing,

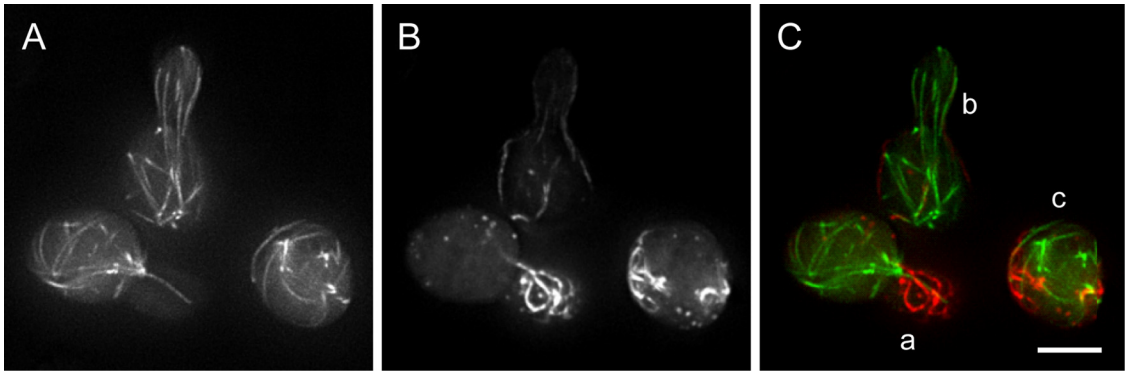

FIG. 7. F-actin and microtubules show distinct spatial organizations in conidia and germlings. (A) β-Tubulin–GFP signal from the middle section of a group of cells showing the distribution of microtubules. (B) Lifeact-TagRFP signal from the same section showing the F-actin distribution. (C) Merged image of panels A and B showing F-actin in red and microtubules in green. (a) Germling with an F-actin array at the tip but only very few microtubules extending into this region. (b) Germling with microtubules extending into the germ tube tip but with no dense accumulation of F-actin currently present. (c) Distribution of F-actin and microtubules in an ungerminated cell. Bar, 5 μm.

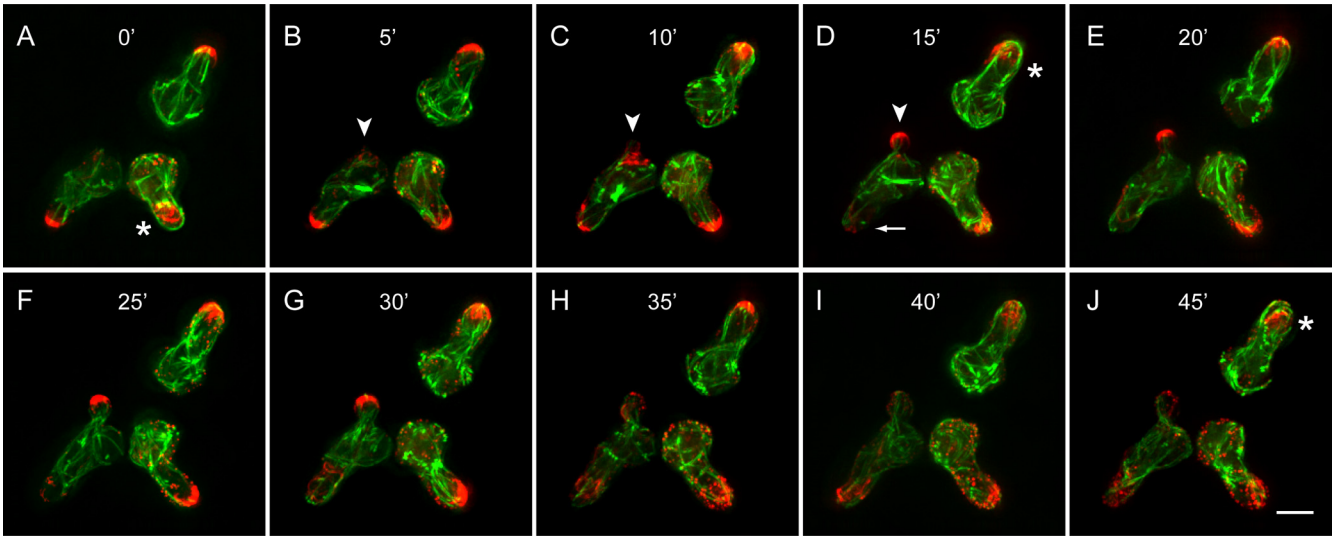

FIG. 8. CAT polarization and protrusion. Microtubules were labeled with β-tubulin–GFP, and F-actin was labeled with Lifeact-TagRFP. (A) Apical F-actin was present at germ tube tips in all three conidial germlings. Over time, these actin caps underwent retrograde movement and dissipation (asterisks) (see Fig. 3 for details). (B) The bottom left germling established a new site of cell polarity, as indicated by the recruitment of F-actin to the cell cortex (arrowhead). (C) Actin array formation coincided with CAT bud emergence. (D) As the CAT elongated, an actin cap formed at its apex. Formation of this CAT coincided with the disappearance of the actin cap in the germ tube tip of the same germling (arrow). (E to J) The CAT extended over the following 10 min but did not elongate beyond 4 to 5 μm in length (E to G), and between 30 and 35 min the actin cap finally disappeared (H to J). (C to H) During the period of CAT formation, germ tube extension was slower (0.04 μm/min) in the germling forming the CAT than in the two germlings that were not forming CATs (0.06 to 0.10 μm/min). CAT elongation, on the other hand, was more rapid (0.14 μm/min). Bar, 5 μm.

pronounced actin arrays were observed only in that one (Fig. 9). Upon contact, actin cables gradually disappeared from the fusion site, which was coincident with the cessation of polarized tip growth. Residual actin cables, however, persisted at the fusion site, suggesting that they may be involved in a later stage of the fusion process. Once cytoplasmic continuity was fully established, actin cables had disappeared from the fused CATs (Fig. 1H and 9H and I), whereas cortical actin patches remained (Fig. 1H). At this stage, germ tube extension resumed, which coincided with the formation of an apical actin array (Fig. 9E, arrowhead). Subsequent to F-actin redeployment, further elongation of the germ tube involved the dynamic re-

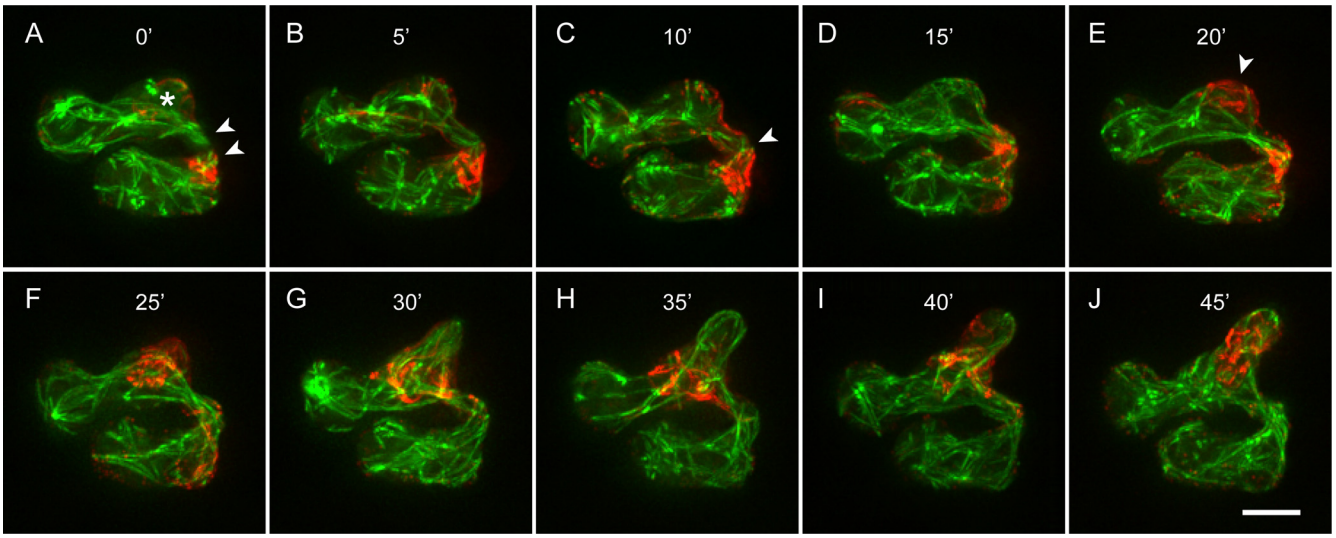

FIG. 9. F-actin dynamics during CAT-mediated cell fusion and germ tube reinitiation. Microtubules were labeled with β-tubulin–GFP, and F-actin was labeled with Lifeact-TagRFP. (A) Two CATs establishing cell-cell contact. The CATs are indicated by arrowheads; the germ tube is indicated by an asterisk. (B to E) Gradual repolarization of F-actin from the fusion site (arrowhead in panel C) to the germ tube tip (arrowhead in panel E). (F to J) F-actin undergoes dynamic rearrangement, while microtubules extend into the growing germ tube. In this instance, germ tube extension increased by a factor of 9 after cell fusion was completed (0.02 μm/min before fusion [A to E] and 0.18 μm/min after fusion [E to J]). Bar, 5 μm.

arrangement of the actin array (Fig. 9G to I). The reinitiation of germ tube growth was also accompanied by extension of microtubules into the tip (Fig. 9G to J).

DISCUSSION

Considerable effort has been expended in attempts to visualize F-actin distribution and dynamics in living fungal cells, and these attempts have mostly relied on fusions between FPs and actin or ABPs (14, 60, 63). The use of FP-actin fusions as reporters for F-actin is problematic, as only a fraction of actin is present in microfilaments, resulting in a low signal-to-noise ratio, and more importantly, the relatively large FP moiety has been shown to perturb actin dynamics in a variety of cell types (2, 43, 62). Thus, FP-actin fusion constructs are likely to alter actin dynamics in filamentous fungi. Fluorescent-protein tagging of ABPs is preferable, as there is generally less perturbation of actin dynamics *in vivo*, but this approach may reveal only a small population of F-actin and the fusion protein may compete with unlabeled endogenous ABPs (11, 61). Therefore, we utilized the Lifeact peptide as a reporter for F-actin in *N. crassa*, which has been shown to provide clear labeling of F-actin in various cell types without interfering with actin dynamics (5, 15, 43, 58, 63). Expression of Lifeact-FP from the *ccg-1* or *tef-1* promoter had no noticeable effect on radial extension rates, cell morphology, germination or cell fusion rates, colony development, or conidiation. The pattern of actin localization revealed by Lifeact-FP was consistent with previous reports on filamentous fungi using immunofluorescence, phalloidin staining, and FP-based live-cell imaging (3, 28, 55, 57) and allowed visualization of F-actin reorganization and polarization in *N. crassa*. Coexpression of Lifeact-TagRFP with β-tubulin–GFP allowed 4D reconstruction of the entire cytoskeleton during early stages of development in living cells of *N. crassa*. To our knowledge, this is the first report of simultaneous visualization of the dynamic interaction of F-actin and microtubules in living fungal cells.

We confirmed the specificity of Lifeact-FP for F-actin with the drug latrunculin A, which prevents F-actin polymerization (6). Treatment with 10 μM Lat A led to a rapid loss of Lifeact-FP-labeled patches and cables, demonstrating a high rate of F-actin turnover in *N. crassa*. Interestingly, although all cables disassembled within 10 min of Lat A treatment, some cables appeared to be initially insensitive to Lat A, implying that different subpopulations of actin cables with different turnover rates exist in *N. crassa*.

In budding yeast, actin cables form tracks for myosin-V-dependent transport of secretory vesicles, whereas actin patches are involved in endocytosis and membrane invagination (34). Both patches and cables localize to new buds in *S. cerevisiae*, but only actin cables are required for polarized secretion (26, 38, 63). The localization of actin patches and cables to the tips of germ tubes and CATs in *N. crassa* suggests active exo- and endocytosis in those regions and indicates a tight coupling of the two processes at this stage of development. Accumulation of actin cables and patches at sites of active growth in *N. crassa* confirms that polarization of the actin cytoskeleton underlies apical extension. Interestingly, the marked differences we observed in F-actin architecture in tip growing regions suggest that the spatial organization of exo- and endocytosis changes during development. A bright focal point of F-actin, colocalizing with the core region of the Spk, and an F-actin-depleted zone followed by a collar of actin patches were present in the tips of mature hyphae compared to the actin arrays and concentration of patches at the extreme apices of germ tubes. The F-actin spot could represent formin-mediated actin nucleation, creating tracks for exocytic vesicles; the formin SepA is found as a spot at hyphal tips that colocalizes with F-actin in *Aspergillus nidulans* (50). In contrast, subapical collars of actin patches are known to be involved in endocytosis in filamentous fungi (3, 57). Thus, it seems the sites of exo- and endocytosis are well separated in mature hyphae while they have tight association in germlings. Extension rates in mature hyphae are 10-fold more rapid than in germlings (4), and the spatial segregation of endocytosis and exocytosis indicates that reorganization of the secretory machinery underlies rapid extension, as has been reported in *Ashbya gossypii* (30).

Consistent with models of actin cable-mediated transport of secretory vesicles in budding yeast, in *N. crassa*, we found that dense arrays of actin cables were present at sites of germ tube emergence and branch formation. Interestingly, cable arrays persisted at the tips of elongating germ tubes and CATs, whereas during branch formation and outgrowth in the mature colony, cables were gradually lost from the tip to be replaced by an F-actin spot and a collar of patches. Lifeact-FP allowed us to monitor the formation of these complex arrays of actin cables during germ tube elongation and to observe their subsequent retrograde movement. This phenomenon was recurrent and was commonly observed during the initial stages of germ tube emergence and elongation but was not observed during branch formation or tip extension in the mature colony. The formation of actin arrays probably represents *de novo* assembly of cables at the tip, eventually leading to backflow of cable arrays. It was possible to observe the movement of a relatively intact array along the length of a germ tube and to monitor its eventual dissolution. It is likely that the disassembly of actin arrays is necessary for reincorporation of the resulting actin subunits into new cables at sites of active growth.

The importance of actin cables for polarized growth is also highlighted by cable localization during and after CAT-mediated cell fusion; dense actin arrays were shown to assemble at the cell cortex prior to CAT formation and to intensify during CAT extension and homing. Shortly after cell fusion, actin cables gradually disappeared from the fusion site while patches persisted. It has been proposed that the polarized secretion of biosynthetic materials is compensated for by endocytosis, maintaining the polarized state of cortical markers and receptors (31, 53, 57). Given the role of actin patches in endocytosis, it is possible that the accumulation of actin patches at the tips of homing CATs and their persistence shortly after fusion facilitates the recycling of membrane receptors and polarity factors no longer required at this site.

Furthermore, Lifeact-FP also showed that actin cables are not always associated with tip growth but have an additional role in septum formation. A formin homolog, SepA, is required for actin ring formation and septation in *A. nidulans*, and it is likely that the *N. crassa* SepA homolog plays a similar role (50). Interestingly, in *N. crassa*, actin rings were formed by the gradual accumulation of preexisting actin cables and their concentration into a ring rather than by *de novo* assembly of

F-actin into a ring. This suggests that ring formation involves both formin-mediated cable production and regulation of the spatial organization of actin cables postproduction.

Coexpression of Lifeact-TagRFP and β-tubulin–GFP revealed distinct but coordinated recruitment of F-actin and microtubules during different stages of cell polarization and tip extension during colony initiation. Previous studies using microtubule-depolymerizing drugs showed that germ tube emergence (but not elongation) can be achieved in *N. crassa* without microtubules (7). Our data showing that polarization of F-actin always preceded polarization of microtubules further reinforces the notion that germ tube emergence and elongation is a two-step process (9, 21) that first involves F-actin to establish a polarized bud and maintain tip polarity but subsequently requires microtubules for further extension. In contrast, CATs are thinner than germ tubes, show determinate growth (45), and do not require microtubules to facilitate cell fusion (46). Consistently, we observed the dynamic rearrangement of actin organization during CAT formation and fusion, suggesting a predominant role for actin in these processes. This notion is supported by findings in *Ustilago maydis*, where it has been demonstrated that cell-cell recognition and cell-cell fusion exclusively depend on F-actin during all stages of polar growth whereas microtubules are required only for long-distance growth of hyphae (19). The function of CATs is to connect cells that are less than 10 to 12 μm apart, i.e., CATs do not need to extend further than 5 to 6 μm. The F-actin cytoskeleton is apparently sufficient to support this short-distance growth and to facilitate fusion. Our observations suggest that recruitment of both cytoskeletal elements occurs in a distinct but coordinated manner and might influence which protrusion is being formed and maintained at any point in time.

Three-dimensional reconstruction and time-lapse microscopy demonstrated a close association of patches and cables (Fig. 1 and 4). Generally, we observed two types of patch behavior: slow/nonlinear and fast/linear movement. Patch formation occurred at the cell cortex and was followed by a short period of undirected movement; then, the patches traveled out of the plane of focus, presumably toward the interior of the cell. The measured velocities and lifetimes of slow/nonlinear patches, 0.26 μm/s and 14 s, respectively, were similar to values obtained for endocytic patches of *A. nidulans* (velocity, 0.19 μm/s; lifetime, 24 s), *Schizosaccharomyces pombe* (velocity, 0.31 μm/s; lifetime, not determined), and *S. cerevisiae* (velocity, 0.1 to 0.5 μm/s; lifetime, 10 to 20 s), and thus, these patches probably represent endocytic vesicles decorated with F-actin (3, 26, 34, 37, 55, 57, 60). Lifeact-FP-labeled patches also underwent directional movement along cables in a discontinuous manner, and occasionally we observed the movement of patches from the cell surface onto actin cables, along which they were transported. These observations strongly indicate that in *N. crassa*, F-actin-decorated endocytic vesicles form at the plasma membrane and, following invagination and scission, can be transported along actin cables. Our observations of patch dynamics in *N. crassa* are consistent with current models of patch formation, which describe how patch movement is correlated with their maturation state (34).

The movement of actin patches along cables has been shown in budding yeast and fission yeast, and in *A. nidulans* actin patches have been shown to undergo linear directed movement along unidentified structures (26, 37, 57). Most interestingly, in *N. crassa*, patches were transported towards and away from the tip, which contrasts with the findings of Huckaba et al. (26), who reported that in budding yeast directional movement of patches along cables is always retrograde to the site of polarized growth. Based on their findings, Huckaba et al. (26) concluded that retrograde patch movement is coupled with the retrograde flow of cables. The saltatory nature and high speed (1.2 μm/s) of actin patch transport along cables in *N. crassa* suggest the involvement of motor proteins (presumably myosins), and the bidirectionality of patch movement implies that F-actin-decorated vesicles can travel toward and away from regions of active growth. The possibility that Lifeact-FP may be labeling "patch-like" structures containing F-actin that are not bona fide endocytic patches should also be considered. Lifeact may be labeling a class of actin-coated microvesicles, termed filasomes (25), that have been shown at the ultrastructural level in fungal hyphae (8, 44).

In conclusion, Lifeact-FP gave clear and robust labeling of F-actin in *N. crassa* without any detectable toxic side effects and provided novel insights into the dynamic reorganization and polarization of the actin cytoskeleton during tip growth and cell fusion. We predict that Lifeact-FP will become a useful tool for studying the regulation, dynamics, and organization of the fungal actin cytoskeleton in the future.

ACKNOWLEDGMENTS

We thank David Kelly from the Centre Optical Instrumentation Laboratory (COIL) at Edinburgh University for help with the DeltaVision system.

Funding for this project was provided by a Biotechnology and Biological Sciences Research Council grant BB/E010741/1 to N.D.R.

REFERENCES

1. **Adams, A., and J. Pringle.** 1984. Relationship of actin and tubulin distribution to bud growth in wild-type and morphogenetic-mutant *Saccharomyces cerevisiae*. J. Cell Biol. **98:**934–945.
2. **Aizawa, H., M. Sameshima, and I. Yahara.** 1997. A green fluorescent protein-actin fusion protein dominantly inhibits cytokinesis, cell spreading, and locomotion in *Dictyostelium*. Cell Struct. Funct. **22:**335–345.
3. **Araujo-Bazán, L., M. A. Peñalva, and E. A. Espeso.** 2008. Preferential localization of the endocytic internalization machinery to hyphal tips underlies polarization of the actin cytoskeleton in *Aspergillus nidulans*. Mol. Microbiol. **67:**891–905.
4. **Araujo-Palomares, C. L., E. Castro-Longoria, and M. Riquelme.** 2007. Ontogeny of the Spitzenkörper in germlings of *Neurospora crassa*. Fungal Genet. Biol. **44:**492–503.
5. **Asakura, T., T. Sasaki, F. Nagano, A. Satoh, H. Obaishi, H. Nishioka, H. Imamura, K. Hotta, K. Tanaka, H. Nakanishi, and Y. Takai.** 1998. Isolation and characterization of a novel actin filament-binding protein from *Saccharomyces cerevisiae*. Oncogene **16:**121–130.
6. **Ayscough, K. R., J. Stryker, N. Pokala, M. Sanders, P. Crews, and D. G. Drubin.** 1997. High rates of actin filament turnover in budding yeast and roles for actin in establishment and maintenance of cell polarity revealed using the actin inhibitor Latrunculin-A. J. Cell Biol. **137:**399–416.
7. **Barja, F., M.-L. Chappuis, and G. Turian.** 1993. Differential effects of anticytoskeletal compounds on the localization and chemical patterns of actin in germinating conidia of *Neurospora crassa*. FEMS Microbiol. Lett. **107:**261–266.
8. **Bourett, T. M., and R. J. Howard.** 1991. Ultrastructural immunolocalization of actin in a fungus. Protoplasma **163:**199–202.
9. **Brand, A., and N. A. R. Gow.** 2009. Mechanisms of hypha orientation of fungi. Curr. Opin. Microbiol. **12:**350–357.
10. **Bretscher, A.** 2003. Polarized growth and organelle segregation in yeast: the tracks, motors, and receptors. J. Cell Biol. **160:**811–816.
11. **Burkel, B. M., G. von Dassow, and W. M. Bement.** 2007. Versatile fluorescent probes for actin filaments based on the actin-binding domain of utrophin. Cell Motil. Cytoskel. **64:**822–832.
12. **Chiu, W., Y. Niwa, W. Zeng, T. Hirano, H. Kobayashi, and J. Sheen.** 1996. Engineered GFP as a vital reporter in plants. Curr. Biol. **6:**325–330.

13. **Davis, R. H.** 2000. *Neurospora*: contributions of a model organism, Oxford University Press, New York, NY.
14. **Doyle, T., and D. Botstein.** 1996. Movement of yeast cortical actin cytoskeleton visualized *in vivo*. Proc. Natl. Acad. Sci. U. S. A. **93:**3886–3891.
15. **Era, A., M. Tominaga, K. Ebine, C. Awai, C. Saito, K. Ishizaki, K. T. Yamato, T. Kohchi, A. Nakano, and T. Ueda.** 2009. Application of Lifeact reveals F-actin dynamics in *Arabidopsis thaliana* and the liverwort, *Marchantia polymorpha*. Plant Cell Physiol. **50:**1041–1048.
16. **Evangelista, M., D. Pruyne, D. C. Amberg, C. Boone, and A. Bretscher.** 2002. Formins direct Arp2/3-independent actin filament assembly to polarize cell growth in yeast. Nat. Cell Biol. **4:**32–34.
17. **Fehrenbacher, K. L., H. C. Yang, A. C. Gay, T. M. Huckaba, and L. A. Pon.** 2004. Live-cell imaging of mitochondrial movement along actin cables in budding yeast. Curr. Biol. **14:**1996–2004.
18. **Fisher-Parton, S., R. M. Parton, P. C. Hickey, J. Dijksterhuis, H. A. Atkinson, and N. D. Read.** 2000. Confocal microscopy of FM4-64 as a tool for analyzing endocytosis and vesicle trafficking in living fungal hyphae. J. Microsc. **198:**246–259.
19. **Fuchs, U., I. Manns, and G. Steinberg.** 2005. Microtubules are dispensable for the initial pathogenic development but required for long-distance hyphal growth in the corn smut fungus *Ustilago maydis*. Mol. Biol. Cell **16:**2746–2758.
20. **Harris, S. D., J. L. Morrell, and J. E. Hamer.** 1994. Identification and characterization of *Aspergillus nidulans* mutants defective in cytokinesis. Genetics **136:**517–532.
21. **Harris, S. D.** 2006. Cell polarity in filamentous fungi: shaping the mold. Int. Rev. Cytol. **251:**41–77.
22. **Heath, I. B., G. Gupta, and S. Bai.** 2000. Plasma membrane-adjacent actin filaments, but not microtubules, are essential for both polarization and hyphal tip morphogenesis in *Saprolegnia ferax* and *Neurospora crassa*. Fungal Genet. Biol. **30:**45–62.
23. **Hickey, P. C., S. R. Swift, M. G. Roca, and N. D. Read.** 2005. Live-cell imaging of filamentous fungi using vital dyes and confocal microscopy, p. 63–87. *In* T. Savidge and C. Pothoulakis (ed.), Methods in microbiology, vol. 34. Elsevier Academic Press, London, United Kingdom.
24. **Honda, S., and E. U. Selker.** 2009. Tools for fungal proteomics: multifunctional *Neurospora* vectors for gene replacement, protein expression and protein purification. Genetics **182:**11–23.
25. **Howard, R. J.** 1981. Ultrastructural analysis of hyphal tip cell growth in fungi: Spitzenkörper, cytoskeleton and endomembranes after freeze-substitution. J. Cell Sci. **48:**89–103.
26. **Huckaba, T. M., A. C. Gay, L. F. Pantalena, H. C. Yang, and L. A. Pon.** 2004. Live-cell imaging of the assembly, disassembly, and actin cable-dependent movement of endosomes and actin patches in the budding yeast, *Saccharomyces cerevisiae*. J. Cell Biol. **167:**519–530.
27. **Karpova, T. S., K. Tatchell, and J. A. Cooper.** 1995. Actin filaments in yeast are unstable in the absence of capping protein or fimbrin. J. Cell Biol. **131:**1483–1493.
28. **Knechtle, P., F. Dietrich, and P. Philippsen.** 2003. Maximal polar growth potential depends on the polarisome component AgSpa2 in the filamentous fungus *Ashbya gossypii*. Mol. Biol. Cell **14:**4140–4154.
29. **Knechtle, P., J. Wendland, and P. Philippsen.** 2006. The SH3/PH domain protein AgBoi1/2 collaborates with the Rho-type GTPase AgRho3 to prevent nonpolar growth at hyphal tips of *Ashbya gossypii*. Eukaryot. Cell **5:**1635–1647.
30. **Köhli, M., V. Galati, K. Boudier, R. W. Roberson, and P. Philippsen.** 2008. Growth-speed-correlated localization of exocyst and polarisome components in growth zones of *Ashbya gossypii* hyphal tips. J. Cell Sci. **121:**3878–3889.
31. **Marco, E., R. Wedlich-Soldner, R. Li, S. J. Altschuler, and L. F. Wu.** 2007. Endocytosis optimizes the dynamic localization of membrane proteins that regulate cortical polarity. Cell **129:**411–422.
32. **Margolin, B. S., M. Freitag, and E. U. Selker.** 1997. Improved plasmids for gene targeting at the *his-3* locus of *Neurospora crassa* by electroporation. Fungal Genet. Newsl. **44:**34–36.
33. **Merzlyak, E. M., J. Goedhart, D. Shcherbo, M. E. Bulina, A. S. Shcheglov, A. F. Fradkov, A. Gaintzeva, K. A. Lukyanov, S. Lukyanov, T. W. Gadella, and D. M. Chudakov.** 2007. Bright monomeric red fluorescent protein with an extended fluorescence lifetime. Nat. Methods **4:**555–557.
34. **Moseley, J. B., and B. L. Goode.** 2006. The yeast actin cytoskeleton: from cellular function to biochemical mechanism. Microbiol. Mol. Biol. Rev. **70:**605–645.
35. **Novick, P., and D. Botstein.** 1985. Phenotypic analysis of temperature-sensitive yeast actin mutants. Cell **40:**405–416.
36. **Pall, M. L., and J. P. Brunelli.** 1994. New plasmid and lambda/plasmid hybrid vectors and a *Neurospora crassa* genomic library containing the bar selectable marker and the Cre/lox site-specific recombination system for use in filamentous fungi. Fungal Genet. Newsl. **41:**63–65.
37. **Pelham, R. J., and F. Chang.** 2001. Role of actin polymerization and actin cables in actin-patch movement in *Schizosaccharomyces pombe*. Nat. Cell Biol. **3:**235–244.
38. **Pruyne, D. W., D. H. Schott, and A. Bretscher.** 1998. Tropomyosin-containing actin cables direct the Myo2p-dependent polarized delivery of secretory vesicles in budding yeast. J. Cell Biol. **143:**1931–1945.
39. **Rasmussen, C. G., and N. L. Glass.** 2005. A rho-type GTPase, *rho-4*, is required for septation in *Neurospora crassa*. Eukaryot. Cell **4:**1913–1925.
40. **Rasmussen, C. G., and N. L. Glass.** 2007. Localization of RHO-4 indicates differential regulation of conidial versus vegetative septation in the filamentous fungus *Neurospora crassa*. Eukaryot. Cell **6:**1097–1107.
41. **Read, N. D., A. Lichius, J. Y. Shoji, and A. B. Goryachev.** 2009. Self-signalling and self-fusion in filamentous fungi. Curr. Opin. Microbiol. **12:**608–615.
42. **Read, N. D., A. Fleißner, M. G. Roca, and N. L. Glass.** 2010. Hyphal fusion. *In* K. A. Borkovich and D. Ebbole (ed.), Cellular and molecular biology of filamentous fungi. ASM Press, Washington, DC.
43. **Riedl, J., A. H. Crevenna, K. Kessenbrock, J. H. Yu, D. Neukirchen, M. Bista, F. Bradke, D. Jenne, T. A. Holak, Z. Werb, M. Sixt, and R. Wedlich-Soldner.** 2008. Lifeact: a versatile marker to visualize F-actin. Nat. Methods **5:**605–607.
44. **Roberson, R. W.** 1992. The actin cytoskeleton in hyphal cells of *Sclerotium rolfsii*. Mycologia **84:**41–51.
45. **Roca, M. G., J. Arlt, C. E. Jeffree, and N. D. Read.** 2005. Cell biology of conidial anastomosis tubes in *Neurospora crassa*. Eukaryot. Cell **4:**911–919.
46. **Roca, M. G., H.-C. Kuo, A. Lichius, M. Freitag, and N. D. Read.** 5 March 2010. Nuclear dynamics, mitosis, and the cytoskeleton during the early stages of colony initiation in *Neurospora crassa*. Eukaryot. Cell doi:10.1128/EC.00329-09.
47. **Sagot, I., S. K. Klee, and D. Pellman.** 2002. Yeast formins regulate cell polarity by controlling the assembly of actin cables. Nat. Cell Biol. **4:**42–50.
48. **Schott, D. H., R. N. Collins, and A. Bretscher.** 2002. Secretory vesicle transport velocity in living cells depends on the myosin-V lever arm length. J. Cell Biol. **156:**35–39.
49. **Shaner, N. C., M. Z. Lin, M. R. McKeown, P. A. Steinbach, K. L. Hazelwood, M. W. Davidson, and R. Y. Tsien.** 2008. Improving the photostability of bright monomeric orange and red fluorescent proteins. Nat. Methods **5:**545–551.
50. **Sharpless, K. E., and S. D. Harris.** 2002. Functional characterization and localization of the *Aspergillus nidulans* formin SEPA. Mol. Biol. Cell **13:**469–479.
51. **Shortle, D., J. E. Haber, and D. Botstein.** 1982. Lethal disruption of the yeast actin gene by integrative DNA transformation. Science **217:**371–373.
52. **Shortle, D., P. Novick, and D. Botstein.** 1984. Construction and genetic characterization of temperature-sensitive alleles of the yeast actin gene. Proc. Natl. Acad. Sci. U. S. A. **81:**4889–4893.
53. **Steinberg, G.** 2007. On the move: endosomes in fungal growth and pathogenicity. Nat. Rev. Microbiol. **5:**309–316.
54. **Suei, S., and A. Garrill.** 2008. An F-actin-depleted zone is present at the hyphal tip of invasive hyphae of *Neurospora crassa*. Protoplasma **232:**165–172.
55. **Taheri-Talesh, N., T. Horio, L. Araujo-Bazán, X. Dou, E. A. Espeso, M. A. Peñalva, S. A. Osmani, and B. R. Oakley.** 2008. The tip growth apparatus of *Aspergillus nidulans*. Mol. Biol. Cell **19:**1439–1449.
56. **Torralba, S., M. Raudaskoski, A. M. Pedregosa, and F. Laborda.** 1998. Effect of cytochalasin A on apical growth, actin cytoskeleton organization and enzyme secretion in *Aspergillus nidulans*. Microbiology **144:**45–53.
57. **Upadhyay, S., and B. D. Shaw.** 2008. The role of actin, fimbrin and endocytosis in growth of hyphae in *Aspergillus nidulans*. Mol. Microbiol. **68:**690–705.
58. **Vidali, L., C. M. Rounds, P. K. Hepler, and M. Bezanilla.** 2009. Lifeact-mEGFP reveals a dynamic apical F-actin network in tip growing plant cells. PLoS One **4:**e5744.
59. **Virag, A., and A. J. Griffiths.** 2004. A mutation in the *Neurospora crassa* actin gene results in multiple defects in tip growth and branching. Fungal Genet. Biol. **41:**213–225.
60. **Waddle, J. A., T. S. Karpova, R. H. Waterston, and J. A. Cooper.** 1996. Movement of cortical actin patches in yeast. J. Cell Biol. **132:**861–870.
61. **Washington, R. W., and D. A. Knecht.** 2008. Actin binding domains direct actin-binding proteins to different cytoskeletal locations. BMC Cell Biol. **9:**10.
62. **Wu, J. Q., and T. D. Pollard.** 2005. Counting cytokinesis proteins globally and locally in fission yeast. Science **310:**310–314.
63. **Yang, H. C., and L. A. Pon.** 2002. Actin cable dynamics in budding yeast. Proc. Natl. Acad. Sci. U. S. A. **99:**751–756.
64. **Yokoyama, K., H. Kaji, K. Nishimura, and M. Miyaji.** 1990. The role of microfilaments and microtubules in apical growth and dimorphism of *Candida albicans*. J. Gen. Microbiol. **136:**1067–1075.